Respiratory Physiology & Neurobiology 265 (2019) 141–152

Contents lists available at ScienceDirect

Respiratory Physiology & Neurobiology

journal homepage: www.elsevier.com/locate/resphysiol

Probing the function of glycinergic neurons in the mouse respiratory network using optogenetics

Michal G. Fortuna[a,b,e,*], Sebastian Kügler[a,c], Swen Hülsmann[a,b,d,**]

[a] DFG Research Center for Nanoscale Microscopy and Molecular Physiology of the Brain (CNMPB), Göttingen, Germany
[b] Institute for Neurophysiology and Cellular Biophysics, Georg-August-University Göttingen, Humboldtallee 23, D-37073 Göttingen, Germany
[c] University Medicine Göttingen, Department of Neurology, 37099 Göttingen, Germany
[d] Clinic for Anesthesiology, University Hospital Göttingen, 37099 Göttingen, Germany
[e] Cognitive Neuroscience Laboratory, German Primate Center, 37077 Göttingen, Germany

ARTICLE INFO

Keywords:
Brainstem
Respiratory pattern generator
Inhibitory neurons
Glycine
Optogenetics

ABSTRACT

Glycine is a primary inhibitory transmitter in the ventral medullary respiratory network, but the functional role of glycinergic neurons for breathing remains a matter of debate. We applied optogenetics to selectively modulate glycinergic neuron activity within regions of the rostral ventral respiratory column (VRC). Responses of the phrenic nerve activity to the light-driven stimulation were studied in the working heart-brainstem preparation from adult glycine transporter 2 Cre mice (GlyT2-Cre), which received a unilateral injection of a Cre-dependent AAV virus into Bötzinger and preBötzinger Complex. Sustained light stimulation from the ventral medullary surface resulted in a substantial depression of the phrenic nerve (PN) frequency, which in most cases was compensated by an increase in PN amplitude. Periodic, burst stimulation with variable intervals could alter and reset respiratory rhythm. We conclude that unilateral activation of the rostral VRC glycinergic neurons can significantly affect respiratory pattern by lengthening the expiratory interval and modulating phase transition.

1. Introduction

Located in the brainstem, the neuronal network controlling breathing provides robust oscillatory motor output coordinating inspiration and expiration. In response to changing metabolic demands (i.e., sleep, exercise), voluntary behavior (i.e., phonation) or to facilitate protective reflexes (i.e., pulmonary reflexes, cough), this circuit must be sufficiently flexible to allow rapid changes in breathing pattern. A critical component of neural circuitry for breathing in mammals is located in the ventrolateral medulla oblongata and is arranged in bilateral columns (e.g., (Alheid et al., 2002; Feldman et al., 2013; Lindsey et al., 2012; Smith et al., 1989)). These columns are roughly organized into functional compartments that subserve inspiration (preBötzinger complex) and expiration (Bötzinger complex) (Richter and Smith, 2014; Smith et al., 2013, 2007; Smith et al., 1991).

The preBötzinger complex (preBötC) contains a population of excitatory pre-inspiratory/inspiratory neurons (pre-I/I) some of which possess intrinsic pace-making properties, and inhibition or selective lesion of this area eliminates breathing *in vivo* (Koshiya and Smith, 1999; Paton et al., 2006; Rekling and Feldman, 1998; Smith et al., 1991; St-John et al., 2009; Tan et al., 2008). However, the preBötC also contains inhibitory inspiratory neurons (early-I), many of which are glycinergic (Koizumi et al., 2013; Morgado-Valle et al., 2010; Winter et al., 2009). Adjacent to the preBötC is the Bötzinger complex (BötC), which has been implicated in the control of expiration and harbors primarily expiratory decrementing (dec-E, also termed post-inspiratory or post-I) and expiratory augmenting neurons (aug-E). Post-I/dec-E neurons are predominantly glycinergic as they expressed glycine transporter-2 (GlyT2) mRNA (Ezure et al., 2003) whereas aug-E neurons may be GABAergic (Champagnat et al., 1982; Haji et al., 1992; Schmid et al., 1996) or glycinergic (Ezure et al., 2003; Fortuna et al., 2008; Schreihofer et al., 1999); this variation may reflect different sub-

Abbreviations: 7 N, facial motor nucleus; 12 N, hypoglossal nucleus; AAV, adeno-associated virus; Amb, nucleus ambiguous; ChAT, choline acetyltransferase; ChR2, channelrhodopsin 2; DMX, also 10 N, dorsal motor nucleus of the vagus nerve; aug-E, expiratory augmenting; dec-E, expiratory decrementing; early-I, early inspiratory; EYFP, enhanced yellow fluorescent protein; GlyT2-Cre, glycine transporter 2 - Cre; IBI, interburst interval; lRt, intermediate zone reticular formation; MPB, medial parabrachial; NTS, the nucleus of the solitary tract; PFA, paraformaldehyde; pfRG, parafacial respiratory group; PN, phrenic nerve; VGlut2, vesicular glutamate transporter 2; VRC, ventral respiratory column; VRG, ventral respiratory group

* Corresponding author at: Cognitive Neuroscience Laboratory, German Primate Center, Kellnerweg 4, 37077 Göttingen, Germany.
** Corresponding author: Clinic for Anesthesiology, University Hospital Göttingen, Humboldtallee 23, 37073 Göttingen, Germany.
E-mail addresses: mfortuna@dpz.eu (M.G. Fortuna), shuelsm2@uni-goettingen.de (S. Hülsmann).

https://doi.org/10.1016/j.resp.2018.10.008
Received 5 March 2018; Received in revised form 23 October 2018; Accepted 31 October 2018
Available online 03 November 2018
1569-9048/

populations of aug-E neurons or co-expression of glycine and GABA. Most models of the respiratory pattern generator assume an essential role of these neurons located in BötC and preBotC in the generation of three phases breathing rhythm (Del Negro et al., 2018; Feldman and Kam, 2015; Richter, 1982; Richter and Smith, 2014: Ausborn et al., 2018; Rybak et al., 2007). Yet, the ultimate role of synaptic inhibition in respiratory rhythm generation remains intensely debated (Del Negro et al., 2018; Feldman et al., 2013; Marchenko et al., 2016; Ramirez and Baertsch, 2018; Ramirez et al., 2012; Richter and Smith, 2014; Smith et al., 2013).

Glycinergic inhibition is believed to be critical for the inspiration to post-inspiration, and late-expiration to inspiration phase transitions (Ausborn et al., 2018; Richter and Smith, 2014; Rybak et al., 2007; Shevtsova et al., 2014). Systemic or local pharmacological blockage of the glycinergic transmission within the ventral respiratory columns, was shown to disrupt the rhythm, de-stabilize the regularity and pattern of inspiration, and abolish post-I motor activity (Bongianni et al., 2010; Busselberg et al., 2001; Dutschmann and Paton, 2002a, b; Paton and Richter, 1995; Pierrefiche et al., 1998; Schmid et al., 1991). However, this view was challenged by Janczewski and colleagues, who showed that postsynaptic inhibition within the preBötC and BötC had little, if any, effect on the rhythm in vagotomised rats (Janczewski et al., 2013). Likewise, the "burstlet hypothesis" assumes the generation of the breathing rhythm without an essential role of inhibitory neurons (Del Negro et al., 2018; Feldman and Kam, 2015).

Recent studies, in which the function of inhibitory neurons was also probed with optogenetics, have found them to be necessary for the inspiratory pattern formation, albeit, reaching different conclusions about the role in the generation of the rhythm *per se* (Ausborn et al., 2018; Baertsch et al., 2018; Sherman et al., 2015). In these studies, bilateral manipulations of the inhibitory neurons were performed, whereas, we took a different approach. By transducing and stimulating neurons unilaterally, we aimed to interfere with glycinergic neurons without completely disrupting the bilaterally located rhythm-generating core of the network. Some results of this work have been presented in an abstract form (Fortuna et al., 2014).

2. Materials and methods

2.1. Animal ethics

Breeding and handling of adult GlyT2-Cre (Tg(Slc6a5-icre)^{121Veul}) (Ishihara et al., 2010) and experiments were performed in compliance with the guidelines for the welfare of experimental animals issued by the European Communities Council Directive (86/609/EEC) and the laws of the Federal Government of Germany. In accordance with the German Protection of Animals Act (Tierschutzgesetz; TierSchG), all procedures were approved by State authorities and the Animal Welfare Office of University Medical Center Göttingen, Germany (33.14-42502-04-1 1/0577 and 33.12-42502-04-14/1524).

2.2. Stereotactic virus injection

For selective transduction of glycinergic neurons, we used the double floxed pAAV-EF1α-DIO-hChR2(H134R)-EYFP-WPRE-HGHpA construct (Addgene, Inc.), which allows Cre-mediated recombination and enables cell type specific ChR2-EYFP expression. AAV6 viruses were generated by the Viral Vectors Laboratory at the Universitätsmedizin Göttingen as described earlier (Kugler et al., 2003). The final virus titer was 0.8×10^8 TU/µl and for injections typically diluted 1:1 with PBS.

Adult male and female GlyT2-Cre mice (average weight 29.6 g, ranging from 19 g to 39 g) received Metamizole (Serumwerk Bernburg AG) in the drinking water 2-days before surgery (0.4 ml in 500 ml), and 2–3 days post-surgery (0.8 in 500 ml). Anesthesia was induced by intraperitoneal injection of Ketamine (80 µg/g body weight), Xylazine (20 µg/g) and Acepromazine (2 µg/g) mix. After induction of anesthesia (lack of paw withdrawal reflex), mice heads were shaved and skin was cleaned with an antiseptic agent (Braunol®, B.Braun Melsungen AG). Animals were placed in the stereotaxic apparatus (Stoelting, Mouse Stereotaxic Instrument) that was motor controlled by" Stereodrive" software (Neurostar, Tübingen). Eye ointment was applied and the temperature was maintained at 37 °C with a servo-controlled heating pad (CMA/150; CMA Microdialysis, Stockholm, Sweden). A small incision was made in the skin, exposed skull cleaned from connective tissue and a burr hole was drilled in the occipital plate.

Virus solution was delivered through a glass pipette (25–35 µm outside diameter at the tip) connected to a pressure injector FemtoJet (Eppendorf). Mice typically received two separate pressure injections of about 200 nl each (150–250 nl, judged by the movement of the meniscus) over a period of 10–15 min each. One injection was centered in BötC and second in the rostral preBötC region, based on the Paxinos and Watson. Stereotaxic coordinates were 1.1 mm lateral, 5.5–5.8 mm ventral with 2.2–2.3 mm caudal to lambda for the Bötzinger Complex and 2.6–2.7 mm caudal to lambda, for the preBötzinger Complex (Paxinos et al., 2001). After the injection, the glass pipette was slowly retracted; brain surface carefully washed with sterile saline before the skin was sutured. Mice were placed in a warm cage until recovered from the surgery and then kept for 2 to 4 weeks post-surgery (24 ± 4.5 days after, except two animals which were used 10 and 12 weeks after initial surgery) to allow for ChR2-EYFP transgene expression.

2.3. In situ arterially perfused brainstem–spinal cord preparation

Electrophysiological experiments were performed using the *in situ* arterially perfused brainstem-spinal cord preparation described earlier (Manzke et al., 2010; Paton, 1996). Mice were heparinized (1250 units, given i.p.) and subsequently deeply anesthetized with isoflurane (soaked surgical gauze in a sealed container) until loss of their paw withdrawal reflex. After sub-diaphragmatically transection, the upper body part was immersed in ice-cold and oxygenated aCSF solution, the skull was opened and the forebrain removed (precolliucular decerebration). Skin, diaphragm, and lungs were removed; the descending aorta and thoracic phrenic (PN) nerve were isolated and cut distally. To access the ventral surface of the medulla, preparation was placed supine, carotid artery and vagus nerve on the side of injection were ligated and cut, the trachea and esophagus were removed. All muscle and connective tissue covering the basilar surface of the occipital bone were removed. The bone was carefully removed using a micro-Rongeur (Fine Science Tools Inc.) to expose the ventral surface of the medulla from the vertebral arteries to the pontine nuclei. In the recording chamber, a small catheter was inserted into the descending aorta for retrograde perfusion by a peristaltic roller pump (Watson Marlow). The perfusion solution consisted of carbogenated (95% O_2, 5–8% CO_2) aCSF at 32 °C with an oncotic agent (Ficoll 1.25%; Sigma). The second lumen of the catheter was used to monitor perfusion pressure. During the initial "tuning phase", a speed of the perfusion was adjusted between 16 and 20 ml min^{-1} (dependent of the weight of the animal) and experiments were started after steady rhythm could be recorded. As slight manipulations of the perfusion conditions could result in alterations of the PN frequency and amplitude (Stettner et al., 2007), we exploited this fact to obtain different respiratory output from the same preparation – this manipulation was successful in 5 experiments (one preparation had a high-frequency of a phrenic activity from the beginning, thus a total of 6 fast rhythms used for the analysis).

The composition of the aCSF was (in mM): 125 NaCl ; 25 $NaHCO_3$; 2.5 $CaCl_2$; 1.25 $MgSO_4$; 1.25 KH_2PO_4; 5 KCl; 10 glucose, osmolality was 290 ± 5 mOsm/L. In addition, vasopressin (200–400 pM) was added to increase peripheral vascular resistance improving brain perfusion. Phrenic nerve activity (PNA) was recorded using custom-made glass suction electrodes. PNA signals were amplified 12,500 times, band-pass filtered (0.25–2 kHz) and integrated (time constant, 0.03-0.06 s) using a

custom-made amplifier (electronic workshop of the department of physiology, Göttingen). Signals were digitized by a PowerLab 8/30 and stored on a PC using LabChart software (ADInstruments).

A blue 473 nm diode laser (DL-473, Rapp OptoElectronic) was controlled by Master 8 stimulator (A.M.P.I) and connected to a 600 µm fiber optic (Thorlabs, BFH37-600-CUSTOM). Bare end of the fiber was positioned just above the exposed ventral surface of the medulla. Power output used for stimulation was measured (PM100 A Compact Power Meter Console (Thorlabs)) at the tip of the fiber and was used in the range of 8–16 mW, typically 12 mW; this is equivalent to an intensity of about 40 mW/mm^2 at the surface of the tissue. Relevant neurons of the preBötC and BötC are located within 300–600 µm from the ventral medullary surface in a mouse, and light transmission drops to about 10% in this rage (Aravanis et al., 2007). If we assume that neurons can be reliably activated if the intensity is above 1 mW/mm^2, sufficient activation of neurons ventral to Nucleus Ambiguus would be reached.

2.4. Tissue fixation for immunohistochemistry

For detailed histological analysis, mice were deeply anesthetized mice with isoflurane (see above). The chest was opened, diaphragm cut and the heart exposed. Mice were perfused transcardially with 50 ml of PBS followed by 100 ml of freshly prepared 4% paraformaldehyde in PBS, pH 7.4. Brains were removed and stored in the perfusion fixative at 4 °C before being cut into 33-µm-thick coronal slices. Tissue was kept in cryoprotectant solution (20% glycerol plus 30% ethylene glycol in 50 mM phosphate buffer, pH 7.4) at −20 °C until processed. Immunohistochemistry was performed on free-floating sections which were washed 3 times in TBS, and subsequently blocked with 10% normal donkey serum with 0.1% Triton-X for 1 h in RT. Sections were then incubated with primary antibodies against (i) GFP/EYFP (Invitrogen, rabbit, dilution 1:2000, for 1 h at RT); (ii) Choline acetyltransferase (ChAT) (Chemicon, goat, diluted 1:500, o/n at 4 °C), or (iii) the vesicular glutamate transporter 2 (VGluT2) (Millipore, guinea pig, diluted 1:1500, o/n at 4 °C). This was followed with three washes, and secondary antibody incubation with (i) Alexa 647-labeled donkey anti-goat (1:250; 1 h RT), Alexa 488 donkey anti-rabbit (1:250; 1 h RT) or Cy3 donkey anti-guinea pig (1:300; 1 h RT). All secondary antibodies and serum were purchased via Dianova from Jacksons ImmunoResearch Laboratories Inc. Finally, sections were washed, mounted on glass slides, dried o/n and coverslipped with DPX (Sigma). Confocal images were taken by an LSM 510 Meta (Zeiss, Oberkochen, Germany).

2.5. Histology from WHBP experimental cases

To assess the extent of transduction in animals used for the *in situ* procedure, brainstems were isolated after the experiment and submerged in 4% paraformaldehyde in PBS and allowed 2 weeks for fixation. Tissue was cut into 35-µm-thick coronal slices, washed, and 1 every 5 sections were mounted on a glass slide, dried overnight (o/n) and coverslipped with DPX (Sigma). The extent of native ChR2-EYFP expression in the lower medulla was examined and mapped with Axio Imager M2 microscope (Zeiss) controlled by Neurolucida software (MBF Bioscience). Note, that the brainstem tissue after *in situ* experiment and fixation-by-diffusion allowed us only to map the general extent of native fluorescence, as cellular morphology was largely unsuitable for more detailed immunohistochemistry. Boundaries between transfected cells bodies and their extensive processes became difficult to demarcate in some instances; thus only rough fluorescence area was traced in most of the cases. Consequently, many outlines in Fig. 1 encompass not only the immediate location of transfected cell bodies (which were mainly found ventral and around the Amb) but also primary fluorescing projections (mostly extending dorsal to the Amb, in the direction of premotor area lRt and hypoglossal nucleus; see also Fig. 3A).

2.6. Data analysis

Analysis of PNA frequency, amplitude, and timing was performed by the analysis function of the LabChart software (ADInstruments) or with Clampfit (Molecular Devices). For further data analysis, Microsoft Excel (Redmond, WA) and SigmaPlot (Systat Software, San Jose, CA) was used. Results are expressed as a mean ± standard error. For statistical analysis of the sustained stimulation (Figs. 4 and 5) One Way RM ANOVA (normality test : Shapiro-Wilk) or One Way RM ANOVA on Ranks followed by All Pairwise Multiple Comparison Procedure (Holm-Sidak method or Tukey Test respectively) were used and differences were considered significant if $p < 0.05$. For the statistical comparison of burst stimulation (respiratory frequency, interbusrts interval and coefficient of variance; Figs. 6 and 7, paired *t*-test was used (normality test: Shapiro-Wilk).

For calculations of inspiratory and expiratory duration before and during sustained stimulation, the built-in function of peak analysis from LabChart software was used. For consistent PND duration (Ti) measurements (independent of the noise level or varying quality of the signal), we used “time interval from first to last crossing of 10% of the height”. Expiratory duration was calculated as “respiratory period minus Ti”. Values were statistically compared by paired *t*-test. (Normality test: Shapiro-Wilk).

2.7. Stimulation analysis

Sustained stimulation was repeated at least 3 times for each preparation (from 3 to 11 repeats, average 4.9 repeats per case, n = 14). Mean PND activity (frequency and amplitude) for each test period (i.e., baseline, stimulation, and recovery) was obtained from LabChart analysis software. Multiple repeats were averaged in Microsoft Excel and reported as mean responses for each preparation (e.g., Fig. 4B1). Data were statistically compared by One Way RM ANOVA.

For periodic stimulation analysis, PNA was recorded along cyclic stimulation trigger (occurring every 2, 3, 4 s, etc., for each separate routine, also during baseline period) and the time from the beginning of each cycle to the peak of succeeding PND was measured. These individual time periods were later expressed as an angle (where 2, 3, or 4 s = 360°, respective to the cycle duration), and plotted on the circular diagram. In this depiction, each dot represents a time point at which PND peaked after the light stimulus onset.

For 17 bust stimulation runs, from 6 experiments, mean PND rate for each period was calculated and compared (presented in Fig. 6E), while individual PND peak-to-peak time measurements were averaged for a duration of a given run, to calculate PN interburst interval and coefficient of variance (shown in Fig. 6 F/G). Statistically compared by paired *t*-test.

3. Results

3.1. Distribution of AAV-6 transduced neurons in the ventral respiratory column

The extent of ChR2-EYFP expression in the GlyT2-Cre mice in the medulla was assessed from brainstems after the electrophysiological experiments (see methods for details). Virus injections were targeted at glycinergic population located in the rostral part of the VRC and were mapped in relation to motor neuron pools (facial motor nucleus - 7 N, nucleus ambiguous - Amb and, hypoglossal nucleus – 12 N), the inferior olive and the pyramidal tract as shown in Fig. 1 using Neurolucida®. ChR2-EYFP expression was primarily found in a region of ventral medulla from the level of the caudal facial nucleus (Bregma −6.5 mm) to the ventral respiratory group (rVRG) (Bregma −7.2 mm; Fig. 1), with dens fluorescent processes within the VRC and extending into the dorsal aspects of the respiratory column. The bulk of the EYFP-positive cells were located around the nucleus ambiguus (Amb, pars compacta),

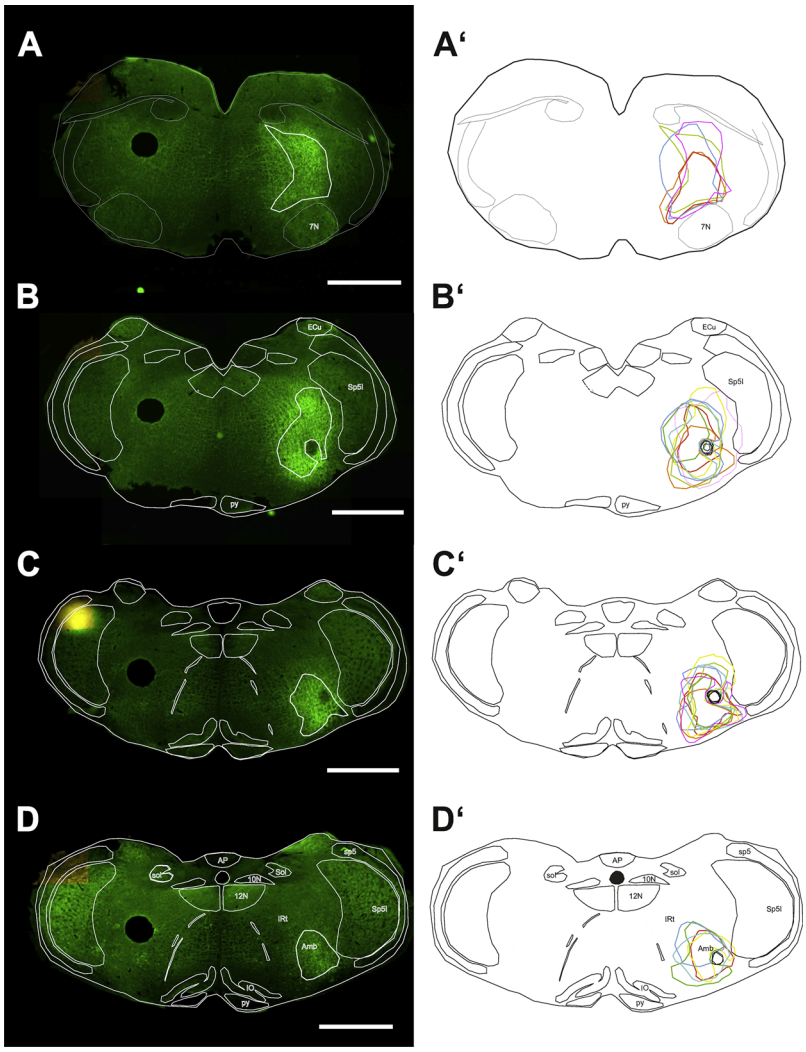

Fig. 1. Virus injection sites and ChR2-EYFP expression in the lower medulla.
Neurolucida-assisted reconstruction of the ChR2-EYFP expression in the lower medulla in relation to anatomical landmarks; the maps represent an overlay of individual experimental cases, that were analyzed in the WHBP and post fixed in PFA after the electrophysiological experiment. Amb: ambiguus nucleus, 7 N - facial nucleus, 10 N – dorsal motor nucleus of the vagus, 12 N - hypoglossal motor nucleus, IO - inferior olive. ECu- external cuneate nucleus, lRt - Intermediate Zone Reticular Formation, Sp5l – spinal trigeminal nucleus interpolar part, sp5 - spinal trigeminal tract, AP – area postrerma, sol – nucleus of the solitary tract, py – pyramidal tract. Scale bar 1 mm

ventrally covering the general area of the Bötzinger Complex (Bregma -6.7 mm) and rostral preBötzinger Complex (Bregma −6.9 mm; Figs. 1 and 2A,). In a few cases, EYFP-positive cells also were observed dorsal to the Amb, along the injection pipette tract. However, we did not observe cell bodies expressing ChR2-EYFP in areas that were more than a few hundred micrometers away from the assumed center of injection (Figs. 2 and 3). EYFP-positive cells bodies were not present contralateral to the injection site, in the dorsal or midline medulla, in areas rostral to the caudal edge of the 7 N, or caudal to the rVRG. From this general assessment, we conclude that the AAV-6 virus was not transported retrogradely and the ChR2-EYFP expression was limited to neurons located in the rostral aspects of the ventrolateral medulla, mostly BötC and preBötC and their immediate surrounding.

ChR2-EYFP- expressing cells displayed extensive dendritic and axonal arborization within the lower medulla ipsilateral to the injection site (Fig. 2A). Fibers crossing the midline were also observed, especially at the level of the hypoglossal nucleus (Figs.2C and 3 A), also innervating contralateral BötC/preBötC (Fig. 2B). Projections of ChR2-EYFP expressing cells included the VRG, Amb area, the nucleus of the solitary tract (NTS), the hypoglossal nucleus along with the adjacent premotor area (lRt; Fig. 3A). Despite dense axonal projections to the hypoglossal nucleus, we did not observe fibers in the dorsal motor nucleus of the vagus nerve (DMX; Figs. 2C & 3 A). EYFP-filled processes could also be seen rostrally to the BötC at the level of the facial nucleus and pfRG (Figs. 1A, 3 B) and in parabrachial nuclei (Fig. 3D).

Using an antibody against VGluT2, we found that ChR2-EYFP-positive boutons and axons did not colocalize with VGLUT2 (Fig. 3E). We also performed co-staining with a marker for cholinergic motor neurons (Fig. 2 and 3F) and confirmed that there was no co-expression of ChR2-EYFP with ChAT-positive neurons. Therefore, based on the specificity of the GlyT2 promoter (Chalphin and Saha, 2010), the injection location, limited viral spread, projection pattern and lack of co-expression of excitatory markers, we assume that inhibitory neurons in the ventral respiratory column were preferentially transduced with ChR2-EYFP.

3.2. *Effect of activation of rVRC glycinergic neurons in situ*

In all our experiments, laser light was delivered via an optic fiber to the ventral medullary surface with no penetration of the brain parenchyma. With this approach, we first tested the effect of high-frequency stimulation (33 Hz, 15 ms light on-15 ms light off, 45 s duration, 30–55 mW/mm^2 power) on the phrenic nerve activity (PNA; Figs. 4 and 5). The respiratory rate of the PNA varied from preparation to preparation ranging from 20–100 min^{-1}. Preparations with a stable respiratory frequency below 60 bpm had usually displayed higher amplitude of the phrenic nerve discharges (PND), while faster preparations (> 60 bpm) showed comparatively lower amplitude PND (in 5 preparations we recorded these two different modes of respiratory activity during one experiment; see methods for details). Thus, for the subsequent analysis, we divided these two modes of respiratory activity into two groups (Figs. 4 and 5). In both groups, light stimulation

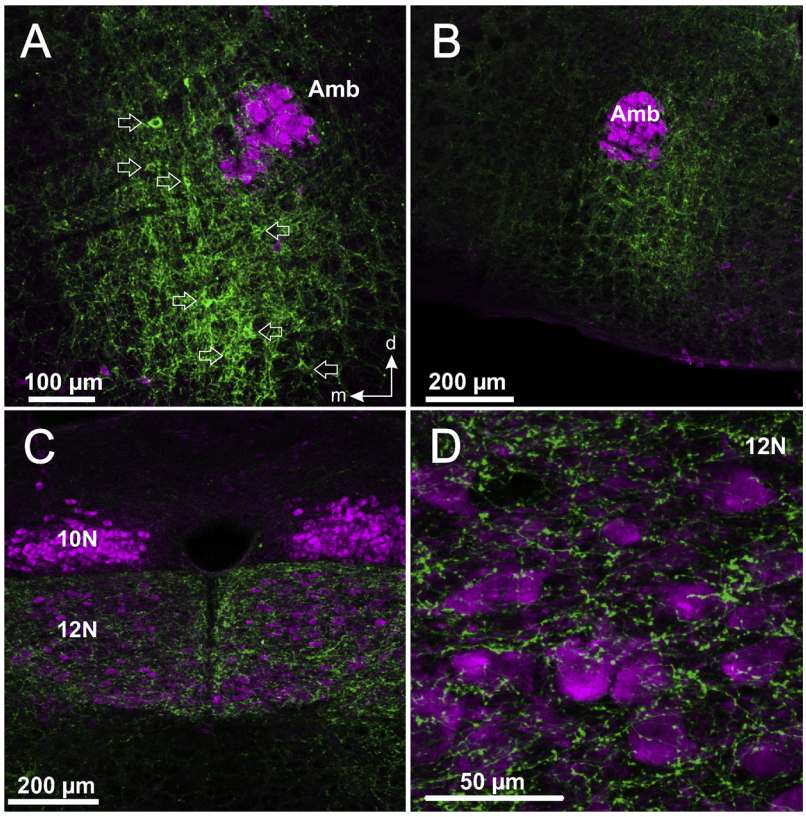

Fig. 2. ChR2-EYFP expression in relation to motor neurons pools. A) Viral transduction in the ventrolateral medulla (side of injection). Note the expression of ChR2-EYFP in neuronal cell bodies ventral and medial to the motor neurons of the nucleus ambiguus (Amb). B) ChR2-EYFP positive projection to the BotC-preBotC area, contralateral to the injection side. C) Innervation of the hypoglossal nucleus (12 N) on both ipsi- and contralateral side of the injection. Note the absence of innervation of motor neurons of the dorsal nucleus of the vagus (10 N). D) Confocal images of the hypoglossal motor neurons apposed by ChR2-EYFP-positve terminals. Motor neurons counterstained with ChAT, and visualized with Alexa 647, pseudo-colored in magenta; EYFP amplified by Alexa 488, pseudo-colored in green. Scale bars shown.

invariably resulted in a reduction of the PND rate. For preparations with a respiratory frequency below 60 bpm (n = 14), PNA dropped by 40% from 30.6 ± 2.7 to 18.0 ± 2.2 bursts.min^{-1} and almost immediately returned to the baseline frequency of 30.1 ± 2.3 bursts.min^{-1} after turning the light off ($p < 0.001$, RM ANOVA; Fig. 4B1, B2). This effect was associated with a modest, yet overall significant increase in the PN amplitude (Fig. 4C1, C2). Although, upon stimulation, inspiratory duration (Ti) increased slightly (from 0.52 s ± 0.08 to 0.56 s ± 0.07, $p = 0.027$), the effect on the expiratory duration (Te) was very pronounced, resulting in an almost doubling of the Te (from 1.70 s ± 0.15 to 3.05 s ± 0.34, $p < 0.001$). Observed effects of light stimulation on the PN amplitude and frequency were much more pronounced in preparations characterized by fast and shallow rhythm – with a stable baseline PND rate above 60 min^{-1} (n = 6). In these cases, continuous light stimulation reduced PND frequency by 60%, from the average of 89.1 ± 3.8 to 34.0 ± 10.6 bursts.min^{-1} ($p < 0.001$, RM ANOVA), which returned to a pre-stimulation activity after the stimulus was removed (Fig. 5A, B1, B2). A very pronounced increase in PN amplitude was observed in this group, with an average 2.60 ± 0.55 fold increase over the baseline value ($p < 0.05$, RM ANOVA; Fig. 5C1, 5C2). Moreover, the effects on Ti and Te were also more dramatic; Ti increased from an average of 0.32 s ± 0.02 to 0.46 s ± 0.03 ($p = 0.002$), whereas Te increased 3.5 times (median = 0.36 s vs. 1.27; $p < 0.05$, Signed Rank Test). Interestingly, as the product of normalized amplitude x frequency was calculated (a correlate of minute ventilation), it became evident that although for individual cases the effects varied (a tendency to either increase or decrease 'minute ventilation' during stimulation), on average there was no significant difference between conditions in each group (Fig. 4D1, D2 and Fig. 5D1, D2; $p = 0.063$ and $p = 0.978$ respectively, RM ANOVA).

3.3. Change of PNA by periodic activation of GlyT2-neurons

In the next set of experiments, we studied the effects of periodic stimulation on the PNA (Figs. 6 and 7). We aimed to test whether periodic activation of glycinergic neurons can reset and/or pace the ongoing respiratory activity. Typically, bursts of light (0.9 s in duration with the same parameters as previously − 33 Hz, 15 ms on/off) were delivered in fixed time intervals, resulting in a light-driven cycle time of 2, 3 or 4 s (e.g. 3 s cycle = 0.9 s light-pulsation + 2.1 light-off) (Fig. 6). Control, free-running PND activity was recorded along the cycle trigger, followed by a periodic light stimulation whose stimulus onset was independent of the phase of the respiratory cycle. Following this protocol, we observed a range of responses in which expiratory duration and transition to inspiration were both affected. Light stimulation typically resulted in PND suppression during the illumination period and subsequent synchronization of the proceeding PND with the light pulse (Fig. 7). Consequently, two general patterns of responses became apparent: (i) extension of the expiratory period by delaying or blocking the upcoming PND (what sometimes resulted in a "rebound burst", reminiscent of a sigh (Fig. 7A)) or (ii) shortening of the expiration by precipitating phase transition, and trigging the next PND burst (which either started to develop in the second half of the light stimulus or developed shortly after (Figs. 6 and 7). Once the phase was reset, successive respiratory cycle did not seem to be affected in terms of duration or pattern and the network was typically generating its baseline rhythm, only to be interrupted by another light burst (Fig. 7A and B).

These general observations were analyzed in more detail from 17 separate stimulation trials (5 × 2 s, 6 × 3 s, 6 × 4 s light-cycle, 0.9 s burst duration) from 6 different preparations characterized by a slower rhythm (mean PN rate 33.7 bpm, range 24–55 bpm). In 9 trials, the frequency was reduced during the period of stimulation (from 9 to 37% of the baseline); in 4 it did not change (mean PND rate within 5% of the baseline), and in 4 there was a slight increase in inspiratory rate (within 5–10% of the baseline rate). The magnitude and type of responses were variable and depended on the endogenous PN rate to the imposed light cycle duration. In 4/5 2 s cycles, PN frequency during stimulation was driven to around imposed 30bpm (1 PND per 2 s cycle); in 4/6 3 s cycles, PN synchronized to the light cycle by either adopting 1:1 rhythm

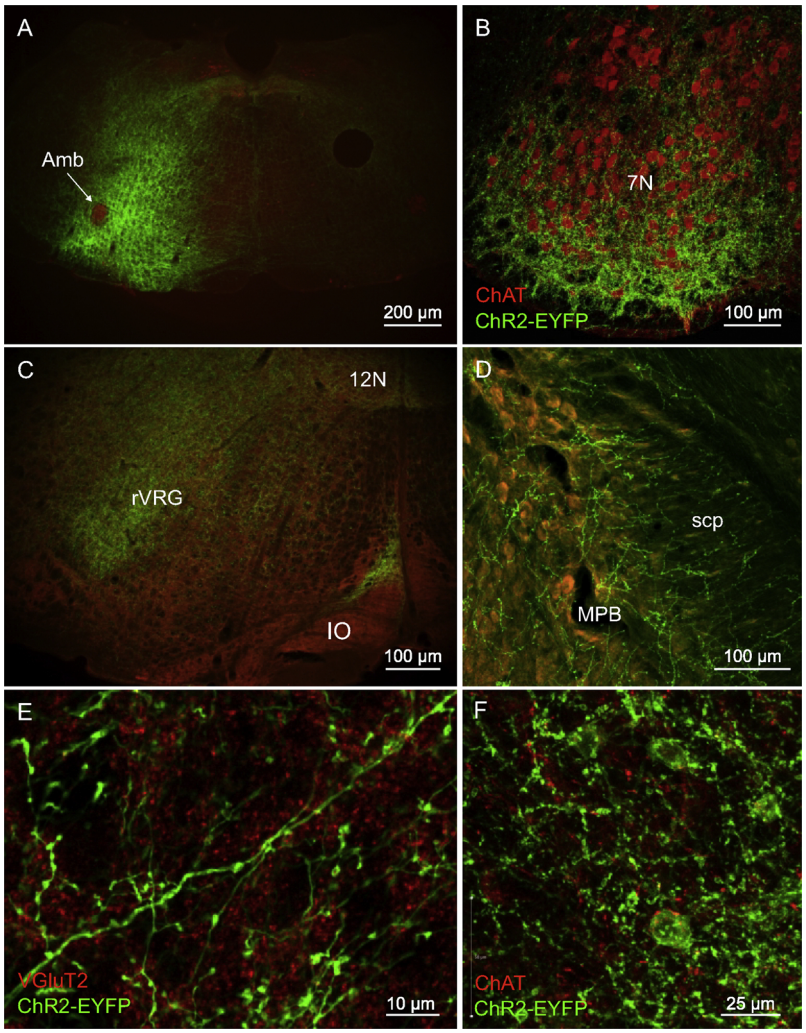

Fig. 3. Projections pattern of inhibitory neurons expressing ChR2-EYFP.

A) Low magnification image of the lower brainstem and expression of ChR2-EYPF (green) after injection of the AAV6 into a BötC - preBötC area in GlyT2-Cre mice; nucleus ambiguus (Amb, in red) is indicated. B) Shows dense projection (green) to the rostral parafacial region, where ChAT-ir motor neurons of the facial nucleus (7 N) are colored in red. C) Axonal projections (green) to respiratory areas in the rostral VRG. D) ChR2-EYFP fibers in medial parabrachial (MPB) area; in pink-red background staining for VGluT2. E) Confocal image of fibers and synaptic boutons in the contralateral rVRG, which do not colocalize with VGluT2 immunoreactivity (red). F) ChR2-EYFP positive neurons on the side of the injection, in the area of nucleus ambiguus; in red ChAT immunoreactive synaptic boutons, which do not colocalize with EYPF positive terminals. Scale bars are shown.

(20 bpm) or 1:2:1:2 rhythm (30 bpm - 2 bursts every second cycle) (Fig. 6A and D); in 4 s cycles, rhythm either synchronized with a light cycle (2 PND bursts per 4 s cycle = 30bpm), or in 3/6 runs did not change and after initial resetting continued at its own pace, without being interrupted by the stimulus. Overall, the respiratory output was adapting to the imposed stimulation cycle (Fig. 7C/D/E), in a way that the mean PND frequency was only marginally decreased (control = 33.7 ± 2.35 bpm vs. stimulation = 29.8 ± 1.85 bpm for all cycle types analyzed, n = 17, p = 0.083) (Fig. 6E). Nonetheless, this adaptation usually was manifested by a less regular rhythm during the stimulation period (1:2:1:2 rhythm or, 2 bursts and a pause during light), characterized by a significant increase in the average PN interburst interval (IBI) (control = 1.92 vs. stimulation = 2.29; p = 0.001, paired t-test; Fig. 6F). A destabilizing effect of the periodic stimulation was also manifested by a marked increase in the IBI coefficient of variance (a measure of relative variability) in 12 out of 17 runs; mean change from 13.5% during control period to 27.3% during stimulation for all 17 runs (p = 0.008, Signed Rank Test) (Fig. 6G). However, in 4 trials there was an apparent reduction in variance, characterized by a rhythm stabilization, tight synchronization of the PND with the light pulse and submission to the impose cycle duration (Fig. 6 A and 7 D). In preparations characterized by a fast rhythm, we did not perform enough repeats to reach statistically supported conclusions, yet in most of the completed runs (9 runs from 3 preparations) light very efficiently blocked the ongoing PNA and reset the rhythm (Fig. 7B and E), sometimes triggering large rebound bursts.

4. Discussion

The current study, performed in the un-anesthetized *in situ* mouse preparation, contributes some new aspects to the ongoing debate about the function of the inhibitory transmission in the generation and modulation of the respiratory rhythm. Utilizing conditional ChR2-expression in GlyT2 neurons of predominately the Bötzinger and preBötzinger Complex, we demonstrate that stimulation of inhibitory neurons on one side only can significantly affect the duration of the respiratory cycle, principally by extending expiratory phase. Moreover, we show these cells can mediate inspiratory-expiratory phase transition and contribute to the maintenance of a stable respiratory output. Despite different levels of baseline activity, optogenetic stimulation of the GlyT2 neurons invariably reduced the frequency of the respiratory rhythm in a fast and reversible manner, an effect, which was usually associated with an increase of the inspiratory amplitude. Our data are in line, with the concept that the inhibitory neurons of the BötC and preBötC are involved in modulation of the ongoing rhythm but not in the rhythmogenesis *per se* (Del Negro et al., 2018; Feldman and Kam, 2015; Janczewski et al., 2013). Thus glycinergic neurons could mediate rapid adjustments of the rhythm and pattern in the face of changing behavior (phonation, swallowing, breath holding, etc.) and during (protective) respiratory reflexes (coughing, sneezing, sigh generation, gasping, Breuer-Hering inflation reflex) (Sherman et al., 2015).

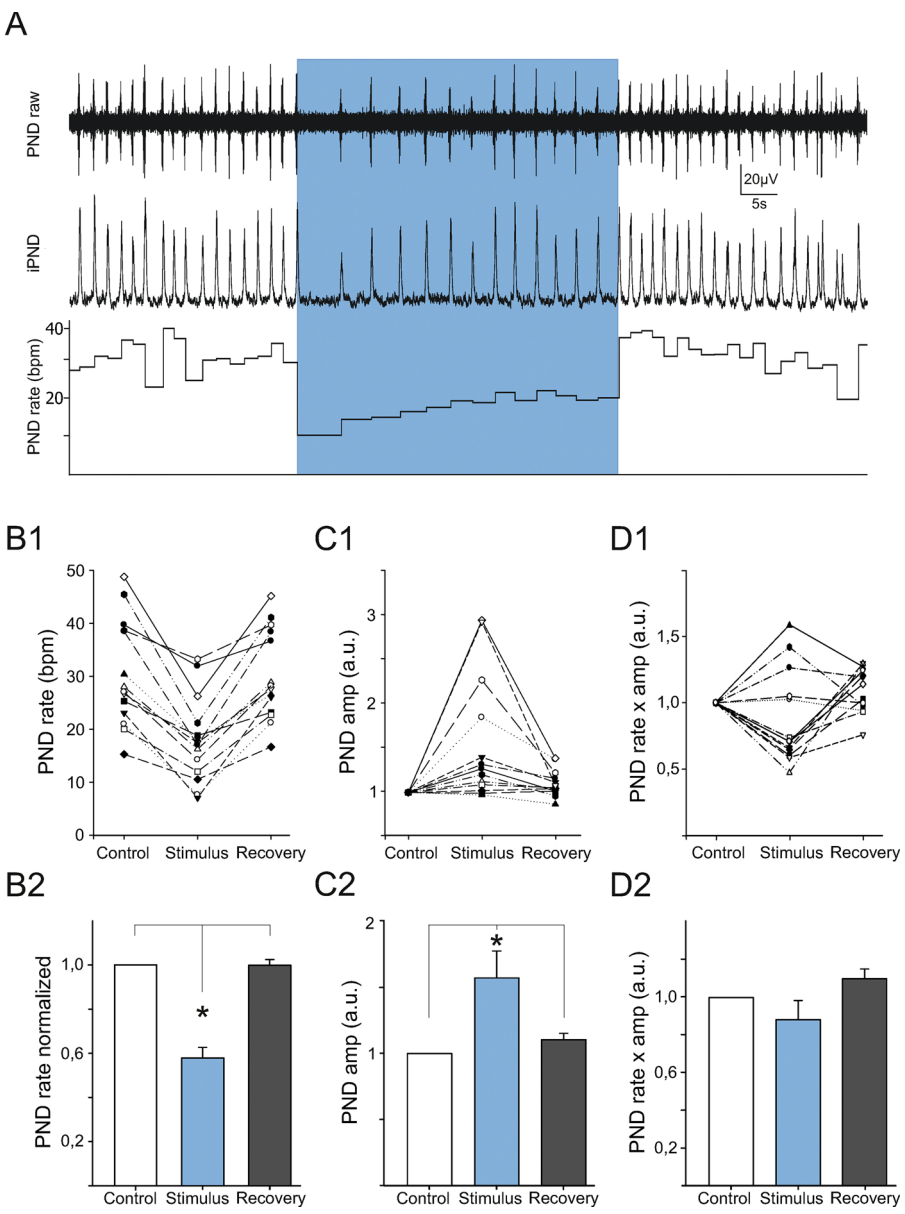

Fig. 4. Effect of continuous light activation on the PNA in slow preparations.
A) Typical response of a phrenic nerve (PN) to a tonic stimulation (33 Hz, 15 ms pulse, 45 s duration) of glycinergic neurons with 473 nm light. Note that PNA quickly recovers to baseline activity after the light is turned off. B1) Individual responses to the stimulation paradigm shown in A. B2) Average response to the stimulation from all the cases shown in B1, $p < 0.001$. C1) Change in PN amplitude for individual experiments during light stimulation. C2) Average change in PN amplitude for all the cases shown in C1, $p < 0.05$. RM ANOVA on Ranks D1) Effects of the stimulation on the product of PN rate x amplitude; variability in the responses is primarily attributed to the difference in the PN amplitude effect, as the PN rate was invariably reduced. D2) Average change in PN rate x amplitude (a.u.) – there was no significant difference between treatments, $p = 0.275$. For B2, and D2 statistical comparison was done by One Way RM ANOVA followed by All Pairwise Multiple Comparison Procedure (Holm-Sidak method). Results are expressed as mean ± standard error.

4.1. Technical considerations

When interpreting these results, one has to consider that the virus injection and the following stimulation was unilateral. Thus, local activation had to be integrated by the unstimulated contralateral compartment, to produce coordinated motor output. Consequently, the effects of *GlyT2*$^+$ neuron activation are most likely more subtle, compared to approaches where bilateral stimulation is applied (Sherman et al., 2015). Secondly, we targeted our viral injections in the rostral VRC to cover both BötC and preBötC. The division between BötC and preBötC is based on histological characterization and their distinct functional properties nevertheless, phenotypically (glycinergic/GABAergic), or functionally alike cells (i.e., dec-E neurons) can be found in both anatomical structures (Alheid and McCrimmon, 2008; Ezure et al., 2003).

Accordingly, we had doubts whether it is feasible to effectively transduce a significant fraction of cells in one area and exclude cells of the same genetic origin in the neighboring area, at least in a mouse. Novel recombinase-based intersectional strategies might be able to overcome these limitations (Dymecki et al., 2010; Hirrlinger et al., 2009). As a consequence, the current observations should be viewed as a result of ChR2-driven enhanced activity of a functionally distinct inhibitory rVRC cells (dec-E, aug-E, and early-I neurons), having in common their genetic identity - an active *GlyT2* promoter (Chalphin and Saha, 2010; Ezure et al., 2003; Schreihofer et al., 1999). Despite relatively small volumes of the virus and limited transduction spread, we cannot exclude that other *GlyT2*$^+$ neurons from the neighboring respiratory related areas (respiratory related cells located dorsal and medial to the Amb, e.g., vlRt glycinergic facial premotor neurons involved in whisking (Moore et al., 2013, 2014), were transduced to a certain degree. This, in combination with a relative strength of the expression in the BötC vs. preBötC respiratory neurons, could account for some of the variability in our results, especially in the cyclic stimulation paradigm.

In the adult mouse brainstem, respiratory neurons of the preBötC and BötC span rostrocaudally for about 800 μm and are mostly located 300–600 μm below the vernal medullary surface (Cui et al., 2016). Power density delivered to the tissue surface in the range of 30 to 55 mW/mm^2 (typically 45 mW/mm^2) decays exponentially to about 10% of the original power when 600 μm deep into the tissue (Aravanis et al., 2007). Assuming that neurons can be reliably activated if the light intensity exceeds 1 mW/mm^2, sufficient activation of neurons

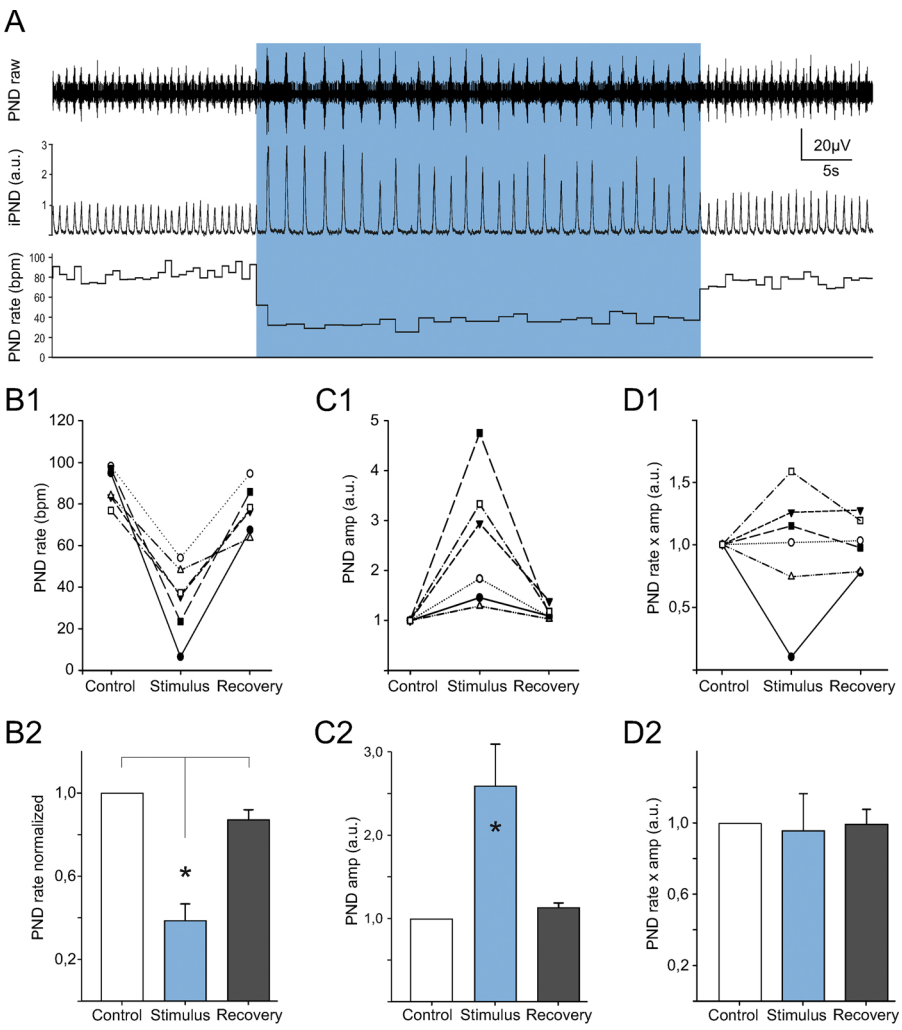

Fig. 5. Effect of continuous light activation on the PNA in fast preparations.
A) Typical response of a phrenic nerve (PN) to a tonic stimulation (33 Hz, 15 ms pulse, 45 s duration) of glycinergic neurons with 473 nm light. Similarly to slow preparations, there was no "after effect" and PNA quickly recovered to control activity after the light stimulus is removed. B1) Individual responses to the stimulation paradigm shown in A; note in one case almost complete apnea. B2) Average response for the cases shown in B1, $p < 0.001$, One way RM ANOVA. C1) Change in PN amplitude in individual cases upon light stimulation; note very large amp increase in half of the cases. C2) Average change in PN amplitude from the cases shown in C1, $p < 0.05$, One way RM ANOVA D1) Effects of the stimulation on the product of PN rate x amplitude D2) Average change in PN rate x amplitude – there was no significant difference between treatments, $p = 0.946$. For B2, C2, and D2 statistical comparison was done by One Way RM ANOVA followed by All Pairwise Multiple Comparison Procedure (Holm-Sidak method). Results are expressed as mean ± standard error.

ventral to Nucleus Ambiguus would be reached (Lin et al., 2009). On the other hand, activation of inhibitory neurons in the medulla located more dorsal to the nucleus ambiguous that are involved in the coordination of breathing with behaviors like chewing, swallowing, vocalization, whisking or eye movement (Moore et al., 2013; Travers et al., 2005; Weber et al., 2015) is less likely (1% initial power when 1 mm deep into the tissue), but cannot be excludes completely. The fact that ChR2 is expressed on all membranes of the cell, including presynaptic terminals, also has to be taken into account. Light stimulation in the region of the preBötC would not only activate ChR2 and trigger synaptic release from neurons whose cell bodies are located within the preBötC itself, but also from those transfected cells and their passing axons which may originate from the BötC or other respiratory-related glycinergic cells, located in proximity and potentially transduced. Therefore, despite limited viral spread, ventral surface illumination and ChR2-EYFP expression predominantly in cells occupying BötC and preBötC, we had to assume that the immediate effect of light stimulation could not be attributed solely to a specific functional compartment or a subpopulation of inhibitory neurons. Since the GlyT2 promoter is specific to glycine releasing neurons (Chalphin and Saha, 2010), the answer of whether glycinergic dec-E (Ezure et al., 2003) or other types of glycinergic neurons or even GABA/glycine co-transmitting neurons (Koizumi et al., 2013; Rahman et al., 2015, 2013) are primarily responsible for observed changes requires different experimental strategies, including detailed immunohistochemistry or more sophisticated genetic models. What can be excluded however, is a direct excitation of the preBötzinger Complex pre-I/I neurons (or motor neuron pools), because we did not observe any co-expression of ChR2-EYFP with makers for excitatory neurons, and in the experiments with phasic stimulation, the delay between the light burst and PND is too long to account for direct pre-I/I glutamatergic activation.

4.2. Stimulation of the glycinergic neurons inhibits respiratory rhythm

The most consistent observation of this study is the inhibition/slowing of the respiratory rhythm upon stimulation of the GlyT2 neurons. This finding could have been expected, considering widely assumed functions of the glycinergic neurons of the BötC (Molkov et al., 2016; Oku and Hulsmann, 2017; Richter and Smith, 2014; Smith et al., 2007). The BötC is known to contain a significant population of expiratory augmenting (aug-E) and expiratory decrementing (dec-E) neurons, which have been shown to be a major source of synaptic inhibition in the respiratory network during expiration (Ezure et al., 2003; Jiang and Lipski, 1990; Richter and Smith, 2014; Schreihofer et al., 1999; Smith et al., 2007). Accordingly, continuous augmentation of the BötC inhibitory activity should result in expiratory period prolongation (prolonged post-inspiratory and late-expiratory phase), in the extreme case leading to apneas. With unilateral stimulation, we saw an average reduction in the respiratory frequency, resulting from extended expiration, by about half during 45 s stimulation protocol (40% in slow and 60% in fast preparations), with the most extended periods of PND suppression at the beginning of the stimulation. We interpret this progressive rhythm accommodation to elevated inhibition as a result of a compensatory drive from the contralateral network, which was not

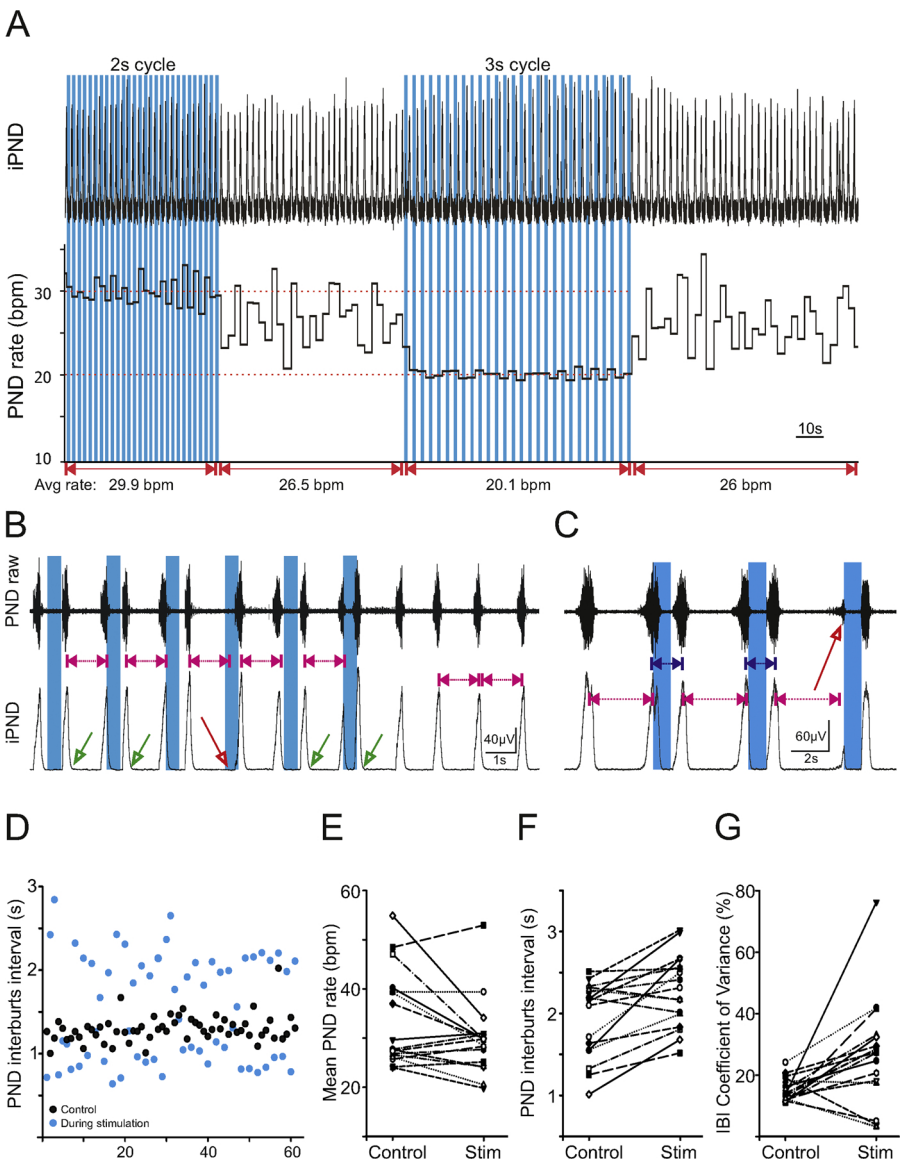

Fig. 6. Effects of periodic light stimulation on the PNA. A) An example of a periodic stimulation paradigm – 0.9 s burst of light (33 Hz, 15 ms on/15off) was delivered in constant time intervals, resulting in fixed light cycle time (e.g., 3 s cycle = 0.9 s light-on + 2.1 light-off); panel illustrates the effect of 2 s and 3 s cycle stimulation on a preparation with a baseline PNA rate of ~26bpm. Note that PNA synchronized with the light and adopted its frequency. B) An example of rhythm disruption by the periodic stimulation (0.45 s in duration in this example); green arrows indicate triggered (premature) PND, and the red arrow points to a delay in PND as a result of stimulation, double-head purple arrows represent interburst interval as measured in control period, ~1.5 s;, we considered a PN burst to be out of phase when the IBI is changed (shortened or extended) by at least 33% of the mean interval measured during the control period. C) A different example showing phase resetting during burst stimulation (1.35 s in duration in this example); red arrow points to the inhibition of the developing PND; note that the light stimulation could block PN only in the early stage of the discharge formation. D) An example of an effect of periodic stimulation on the PN interburst interval; black dots represent individual peak-to-peak time measurements taken during control period, and blue dots during a 3 s cycle stimulation (0.9 s light on + 2.1 s off). E) Mean PN rate before and during periodic stimulation (control = 33.7 ± 2.35 bpm vs. stimulation = 29.8 ± 1.85 bpm for all trials analyzed - 2 s, 3 s and 4 s cycles, 0.9 s stimulus duration, n = 17, p = 0.083); note a tendency for PND rate to group around imposed 30bpm (1 PND per 2 s cycle, and 1:2:1:2 rhythm in 3 s cycle) during stimulation. F) Individual effects of the periodic stimulation on the PND interburst interval (average response: control = 1.92 vs. stimulation = 2.29; p = 0.001, paired t-test). G) Mean PN interburst interval coefficient of variance was significantly increased during periodic stimulation (from 13.5% during control period to 27.3% during stimulation for all 17 runs; p = 0.008 Signed Rank Test); note that in 4 cases coefficient of variance decrease, an effect of PN tightly synchronizing with the imposed light cycle.

stimulated directly. In preparations characterized by a rapid rhythm, the reduction in the frequency was more pronounced, and in some instances, long periods of apneas were observed, only to be interrupted by high amplitude and robust PND (Fig. 5). Importantly, there was no long-lasting effect of the light stimulation (e.g., respiratory ataxia or rhythm desynchronization) and respiratory rhythm very quickly came back to the pre-stimulation activity after turning the light off. We think these results agree with the characteristic of fast synaptic transmission, proposed functions of the glycinergic neurons located in BötC and preBötC and the current models of the respiratory pattern generator (Ausborn et al., 2018; Richter and Smith, 2014; Molkov et al., 2016). Interestingly, comparable observations were reported by Sherman et al. (2015), in awake and anesthetized mouse, yet the authors attribute the effects of the stimulation to the glycinergic neurons of the preBötC.

4.3. Continuous activation of the glycinergic neurons potentiates PN amplitude

The second observation, which on the case-to-case bases was more variable than the rhythm suppression, was the overall increase in the PND amplitude during the light stimulation. This effect was not evident in all the cases (Fig. 4C) and much more pronounced in preparations characterized by the fast and shallow rhythm (Fig. 5C), suggesting that the effect of inhibition on the inspiratory pattern formation might be state dependent. Working-heart brainstem preparations can produce stable respiratory frequency in the range from 21 ± 4.4 bursts.min^{-1} (Paton, 1996) to 171 ± 20 bursts.min^{-1} (Stettner et al., 2008). The resting respiratory rate in awake mice can vary strongly (on average about 160bpm), and especially in periods of intensive sniffing the network can produce respiratory rates above 400 bpm (Hülsmann et al., 2016; Mesuret et al., 2018; Wegener et al., 2014). Currently, it is not known which state of the WHBP is the most comparable to eupneic breathing *in vivo*, and when inhibition might play the most prominent role in coordinating respiratory output. However, it is possible that the variation in PND amplitude responses, irrespective of the baseline activity, resulted simply from a different ratio of transfected neurons in BötC vs. preBötC. Change in relative proportions of neurons activated in the BötC-preBötC network, namely aug-E, dec-E/post-I and early-I, would result in different weights of synaptic input to the excitatory pre-I and ramp-I neurons, resulting in diverse pattern of the PN activity (Oku and Hulsmann, 2017; Richter and Smith, 2014; Smith et al., 2007). An additional respiratory network modeling could provide further arguments for this explanation. Since activation of glycinergic neurons is supposed to hyperpolarize excitatory neurons in the VRC (e.g., pre-I neurons), augmented activation of low threshold depolarization currents, e.g., mediated by I_h (Thoby-Brisson et al., 2000) might

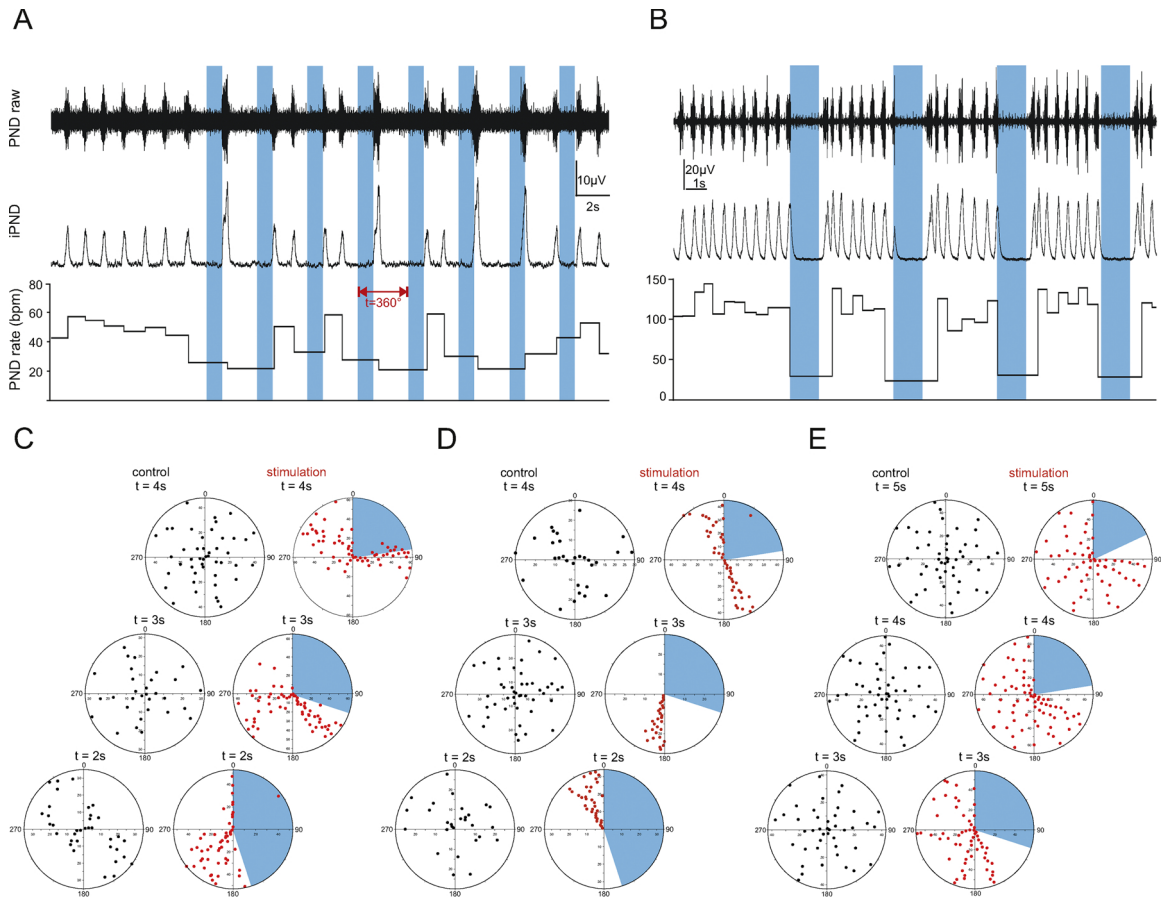

Fig. 7. Effects of periodic light stimulation on the respiratory pattern – a circular analysis.
A) An example of cyclic stimulation in slow oscillating preparation. The time of a full cycle (measured from the beginning of one light burst to of the next one – indicated by red, double-head arrow) is 4 s, and is corresponding to 360° on the circular diagram. The time measured from the start of each cycle to the peak of PND in that cycle is plotted as an angle on the circular diagram (e.g., if a PND peaked 2 s after the beginning of a light burst in a 4 s cycle, this would correspond to a red dot positioned at 180° in the diagram). Note that some of PND that occur after the stimulation resemble sigh. B) An example of periodic activation in fast oscillating preparation – 5 s cycle with 1.35 s light duration shown. C) A circular diagrams depicting the timing of PND occurrence (dots on the diagram, measured as the time from the beginning of the stimulus to the peak of the PND in a given cycle) in relation to the light stimulus (blue area) in the same preparation, during different cycling trials (2, 3 and 4 s). D) A different example is shown, where PND tightly synchronized with the imposed rhythm and occurred in a constant delay in respect to the stimulus. E) An example of circular diagrams generated from fast oscillating preparation (not the same as in B); note, similarly as in B, an effective blockage of the PND during light stimulation and synchronization with the light pulse.

follow and generate synchronized rebound excitation, allowing to overcome the effect of increased inhibition (Bender et al., 2005). Interestingly, augmented bursts that occurred in some experiments during periodic stimulation (Fig. 7A) resembled in some aspects sighs, which have been suggested to require the activity of inhibitory neurons for their generation (Toporikova et al., 2015).

4.4. Periodic glycinergic neuron activation mediates respiratory phase transition

A light-driven burst of glycinergic activation typically resulted in PND suppression during the illumination period and the synchronization of the subsequent PND with the light pulses. Depending on the endogenous PN activity, this resulted in either disruption of the respiratory rhythm or stabilization of the ongoing inspiratory activity, which became paced by the imposed light cycle. These observations support the view that the rVRC glycinergic neurons may play an instrumental role in respiratory phase transition and consequently, their coordinated action is needed to change/reset the rhythm *ad hoc*. This is not to be mistaken with rhythmogenesis, as it has been shown that stable rhythmic output can be generated in the presence of antagonists for GABA and glycine (Janczewski et al., 2013) (but also see (Marchenko et al., 2016) for a different view). The phase resetting might become more critical in mediating protective reflexes like coughing, sneezing, and gasping, as well as in situations when respiratory muscles and ventilation need to be coordinated with behaviors like swallowing, phonation, breathe holding, etc. This interpretation is supported by the observation that the stimulation could both block developing PND (delay inspiration) or trigger a premature PN discharge (advance inspiration) (Fig. 6B and C) and the close proximity and connectivity of the rVRC glycinergic neurons with medullary areas involved in orto-facial control (vlRt, hypoglossal nucleus). Shortening of the respiratory phase duration is in line with very recent findings where activation of inhibitory neurons during ongoing inspiratory activity, shortened the refractory period of excitatory (*dbx*-positive) rhythmogenic neurons and allowed the next respiratory cycle to start earlier (Baertsch et al., 2018).

Challenging ongoing rhythm with out of phase burst of stimulation produced irregular PND pattern marked by increased interburst interval variability. However, the inspiratory output (probably facilitated by the contralateral rhythmogenic network) would typically adapt to the artificial stimulus in a way that would maintain an overall level of ventilation – only slightly reduced mean respiratory rate during stimulation period (Fig. 6D and E). We could observe these rapid adjustments in both types of rhythms (fast and slow), yet again, fast oscillating preparations seemed to be more responsive to the unilateral light

stimulation.

In sum, we conclude that GlyT2$^+$ inhibitory neurons in the VRC have an impact on expiratory-inspiratory phase transition, phase duration and thus respiratory frequency. Since even unilateral activation can delay the development of the next inspiratory burst or induce rebound activation depending on the phase of stimulation, our data is in line with the concept that GlyT2$^+$ inhibitory neurons are actively involved in the reflexes control of breathing.

Acknowledgment

The authors are grateful to A.M. Bischoff for excellent technical assistance with the working heart-brainstem preparation (WHBP), to J. Staiger and R. Wagener (Neuroanatomy Göttingen) for providing access and assistance to the Neurolucida software, and S.B. Abbott (University of Virginia) for critical comments on the manuscript. The study was funded by the Deutsche Forschungsgemeinschaft (grant Hu797/7-1;8-1 to S.H.) and founding from the Cluster of Excellence 171 - DFG Research Center 103 Nanoscale Microscopy and Molecular Physiology of the Brain (CNMPB) to S.H. and S.K.. M.G.F was supported by the Alexander von Humboldt Foundation.

References

Alheid, G.F., Gray, P.A., Jiang, M.C., Feldman, J.L., McCrimmon, D.R., 2002. Parvalbumin in respiratory neurons of the ventrolateral medulla of the adult rat. J. Neurocytol. 31, 693–717.

Alheid, G.F., McCrimmon, D.R., 2008. The chemical neuroanatomy of breathing. Respir. Physiol. Neurobiol. 164, 3–11.

Aravanis, A.M., Wang, L.P., Zhang, F., Meltzer, L.A., Mogri, M.Z., Schneider, M.B., Deisseroth, K., 2007. An optical neural interface: in vivo control of rodent motor cortex with integrated fiberoptic and optogenetic technology. J. Neural Eng. 4, S143–156.

Ausborn, J., Koizumi, H., Barnett, W.H., John, T.T., Zhang, R., Molkov, Y.I., Smith, J.C., Rybak, I.A., 2018. Organization of the core respiratory network: insights from optogenetic and modeling studies. PLoS Comput. Biol. 14, e1006148.

Baertsch, N.A., Baertsch, H.C., Ramirez, J.M., 2018. The interdependence of excitation and inhibition for the control of dynamic breathing rhythms. Nat. Commun. 9, 843.

Bender, R.A., Galindo, R., Mameli, M., Gonzalez-Vega, R., Valenzuela, C.F., Baram, T.Z., 2005. Synchronized network activity in developing rat hippocampus involves regional hyperpolarization-activated cyclic nucleotide-gated (HCN) channel function. Eur. J. Neurosci. 22, 2669–2674.

Bongianni, F., Mutolo, D., Cinelli, E., Pantaleo, T., 2010. Respiratory responses induced by blockades of GABA and glycine receptors within the Botzinger complex and the pre-Botzinger complex of the rabbit. Brain Res. 1344, 134–147.

Busselberg, D., Bischoff, A.M., Paton, J.F., Richter, D.W., 2001. Reorganisation of respiratory network activity after loss of glycinergic inhibition. Pflugers Arch. 441, 444–449.

Chalphin, A.V., Saha, M.S., 2010. The specification of glycinergic neurons and the role of glycinergic transmission in development. Front. Mol. Neurosci. 3, 11.

Champagnat, J., Denavit-Saubie´, M., Moyanova, S., Rondouin, G., 1982. Involvement of amino acids in periodic inhibitions of bulbar respiratory neurones. Brain Res. 237, 351–365.

Cui, Y., Kam, K., Sherman, D., Janczewski, W.A., Zheng, Y., Feldman, J.L., 2016. Defining preBotzinger complex rhythm- and pattern-generating neural microcircuits in vivo. Neuron 91, 602–614.

Del Negro, C.A., Funk, G.D., Feldman, J.L., 2018. Breathing matters. Nat. Rev. Neurosci. 19 (June(6)), 351–367.

Dutschmann, M., Paton, J.F., 2002a. Inhibitory synaptic mechanisms regulating upper airway patency. Respir. Physiol. Neurobiol. 131, 57–63.

Dutschmann, M., Paton, J.F.R., 2002b. Glycinergic inhibition is essential for co-ordinating cranial and spinal respiratory motor outputs in the neonatal rat. J. Physiol. (Paris) 2002 (September 1), 643–653 543(Pt 2).

Dymecki, S.M., Ray, R.S., Kim, J.C., 2010. Mapping cell fate and function using recombinase-based intersectional strategies. Methods Enzymol. 2010 (477), 183–213.

Ezure, K., Tanaka, I., Kondo, M., 2003. Glycine is used as a transmitter by decrementing expiratory neurons of the ventrolateral medulla in the rat. J. Neurosci. 23, 8941–8948.

Feldman, J.L., Del Negro, C.A., Gray, P.A., 2013. Understanding the rhythm of breathing: so near, yet so far. Annu. Rev. Physiol. 75, 423–452.

Feldman, J.L., Kam, K., 2015. Facing the challenge of mammalian neural microcircuits: taking a few breaths may help. J. Physiol. 593, 3–23.

Fortuna, M., Bischoff, A.-M., Kügler, S., Hülsmann, S., 2014. The effect of optogenetic stimulation of the Glycinergic neuronsof the mammalian respiratory network. Acta Physiol. Oxf. (Oxf) 210 OS7-05.

Fortuna, M.G., West, G.H., Stornetta, R.L., Guyenet, P.G., 2008. Botzinger expiratory-augmenting neurons and the parafacial respiratory group. J. Neurosci. 28, 2506–2515.

Haji, A., Takeda, R., Remmers, J.E., 1992. Evidence that glycine and GABA mediate postsynaptic inhibition of bulbar respiratory neurons in the cat. J. Appl. Physiol. 73, 2333–2342.

Hirrlinger, J., Scheller, A., Hirrlinger, P.G., Kellert, B., Tang, W., Wehr, M.C., Goebbels, S., Reichenbach, A., Sprengel, R., Rossner, M.J., Kirchhoff, F., 2009. Split-cre complementation indicates coincident activity of different genes in vivo. PLoS One 4, e4286.

Hülsmann, S., Mesuret, G., Dannenberg, J., Arnoldt, M., Niebert, M., 2016. GlyT2-dependent preservation of MECP2-expression in inhibitory neurons improves early respiratory symptoms but does not rescue survival in a mouse model of Rett syndrome. Front. Physiol. 7, 385.

Ishihara, N., Armsen, W., Papadopoulos, T., Betz, H., Eulenburg, V., 2010. Generation of a mouse line expressing Cre recombinase in glycinergic interneurons. Genesis 48, 437–445.

Janczewski, W.A., Tashima, A., Hsu, P., Cui, Y., Feldman, J.L., 2013. Role of inhibition in respiratory pattern generation. J. Neurosci. 33, 5454–5465.

Jiang, C., Lipski, J., 1990. Extensive monosynaptic inhibition of ventral respiratory group neurons by augmenting neurons in the Botzinger complex in the cat. Exp. Brain Res. 81, 639–648.

Koizumi, H., Koshiya, N., Chia, J.X., Cao, F., Nugent, J., Zhang, R., Smith, J.C., 2013. Structural-functional properties of identified excitatory and inhibitory interneurons within pre-Botzinger complex respiratory microcircuits. J. Neurosci. 33, 2994–3009.

Koshiya, N., Smith, J.C., 1999. Neuronal pacemaker for breathing visualized in vitro. Nature 400, 360–363.

Kugler, S., Lingor, P., Scholl, U., Zolotukhin, S., Bahr, M., 2003. Differential transgene expression in brain cells in vivo and in vitro from AAV-2 vectors with small transcriptional control units. Virology 311, 89–95.

Lin, J.Y., Lin, M.Z., Steinbach, P., Tsien, R.Y., 2009. Characterization of engineered channelrhodopsin variants with improved properties and kinetics. Biophys. J. 96, 1803–1814.

Lindsey, B.G., Rybak, I.A., Smith, J.C., 2012. Computational models and emergent properties of respiratory neural networks. Compr. Physiol. 2012 (July (3)), 1619–1670.

Manzke, T., Niebert, M., Koch, U.R., Caley, A., Vogelgesang, S., Hulsmann, S., Ponimaskin, E., Muller, U., Smart, T.G., Harvey, R.J., Richter, D.W., 2010. Serotonin receptor 1A-modulated phosphorylation of glycine receptor alpha3 controls breathing in mice. J. Clin. Invest.

Marchenko, V., Koizumi, H., Mosher, B., Koshiya, N., Tariq, M.F., Bezdudnaya, T.G., Zhang, R., Molkov, Y.I., Rybak, I.A., Smith, J.C., 2016. Perturbations of respiratory rhythm and pattern by disrupting synaptic inhibition within pre-bötzinger and bötzinger complexes. eNeuro 3 ENEURO.0011-0016.2016.

Mesuret, G., Dannenberg, J., Arnoldt, M., Grützner, A.-A., Niebert, M., Hülsmann, S., 2018. Breathing disturbances in a model of Rett syndrome: A potential involvement of the glycine receptor α3 subunit? Respir. Physiol. Neurobiol. 248, 43–47.

Molkov, Y.I., Rubin, J.E., Rybak, I.A., Smith, J.C., 2016. Computational models of the neural control of breathing. Wiley Interdiscip. Rev. Syst. Biol. Med. 2017 (March (2)). https://doi.org/10.1002/wsbm.1371.

Moore, J.D., Deschenes, M., Furuta, T., Huber, D., Smear, M.C., Demers, M., Kleinfeld, D., 2013. Hierarchy of orofacial rhythms revealed through whisking and breathing. Nature 497, 205–210.

Moore, J.D., Kleinfeld, D., Wang, F., 2014. How the brainstem controls orofacial behaviors comprised of rhythmic actions. Trends Neurosci. 37, 370–380.

Morgado-Valle, C., Baca, S.M., Feldman, J.L., 2010. Glycinergic pacemaker neurons in preBotzinger complex of neonatal mouse. J. Neurosci. 30, 3634–3639.

Oku, Y., Hulsmann, S., 2017. A computational model of the respiratory network challenged and optimized by data from optogenetic manipulation of glycinergic neurons. Neuroscience 347, 111–122.

Paton, J.F., Abdala, A.P., Koizumi, H., Smith, J.C., St-John, W.M., 2006. Respiratory rhythm generation during gasping depends on persistent sodium current. Nat. Neurosci. 9, 311–313.

Paton, J.F., Richter, D.W., 1995. Role of fast inhibitory synaptic mechanisms in respiratory rhythm generation in the maturing mouse. J. Physiol. (Paris) 484, 505–521.

Paton, J.F.R., 1996. A working heart-brainstem preparation of the mouse. J. Neurosci. Methods 65, 63–68.

Paxinos, G., Franklin, K.B.J., Franklin, K.B.J., 2001. The Mouse Brain in Stereotaxic Coordinates. Academic Press, San Diego.

Pierrefiche, O., Schwarzacher, S.W., Bischoff, A.M., Richter, D.W., 1998. Blockade of synaptic inhibition within the pre-Botzinger complex in the cat suppresses respiratory rhythm generation in vivo. J. Physiol. (Paris) 509, 245–254.

Rahman, J., Besser, S., Schnell, C., Eulenburg, V., Hirrlinger, J., Wojcik, S.M., Hulsmann, S., 2015. Genetic ablation of VIAAT in glycinergic neurons causes a severe respiratory phenotype and perinatal death. Brain Struct. Funct. 220, 2835–2849.

Rahman, J., Latal, A.T., Besser, S., Hirrlinger, J., Hulsmann, S., 2013. Mixed miniature postsynaptic currents resulting from co-release of glycine and GABA recorded from glycinergic neurons in the neonatal respiratory network. Eur. J. Neurosci. 37, 1229–1241.

Ramirez, J.M., Baertsch, N.A., 2018. The dynamic basis of respiratory rhythm generation: one breath at a time. Annu. Rev. Neurosci. 2018 (July 41), 475–499.

Ramirez, J.M., Doi, A., Garcia, A.J., Elsen, F.P., Koch, H., Wei, A.D., 2012. The cellular building blocks of breathing. Compr. Physiol. 2.4 (2012), 2683.

Rekling, J.C., Feldman, J.L., 1998. PreBotzinger complex and pacemaker neurons: hypothesized site and kernel for respiratory rhythm generation. Annu. Rev. Physiol. 60, 385–405.

Richter, D.W., 1982. Generation and maintenance of the respiratory rhythm. J. Exp. Biol. 100, 93–107.

Richter, D.W., Smith, J.C., 2014. Respiratory rhythm generation in vivo. Physiol.

Bethesda (Bethesda) 29, 58–71.
Rybak, I.A., Abdala, A.P., Markin, S.N., Paton, J.F., Smith, J.C., 2007. Spatial organization and state-dependent mechanisms for respiratory rhythm and pattern generation. Prog. Brain Res. 165, 201–220.
Schmid, K., Böhmer, G., Gebauer, K., 1991. Glycine receptor-mediated fast synaptic inhibition in the brainstem respiratory system. Respir. Physiol. 84, 351–361.
Schmid, K., Foutz, A.S., Denavit-Saubie, M., 1996. Inhibitions mediated by glycine and GABAA receptors shape the discharge pattern of bulbar respiratory neurons. Brain Res. 710, 150–160.
Schreihofer, A.M., Stornetta, R.L., Guyenet, P.G., 1999. Evidence for glycinergic respiratory neurons: botzinger neurons express mRNA for glycinergic transporter 2. J. Comp. Neurol. 407, 583–597.
Sherman, D., Worrell, J.W., Cui, Y., Feldman, J.L., 2015. Optogenetic perturbation of preBotzinger complex inhibitory neurons modulates respiratory pattern. Nat. Neurosci. 18, 408–414.
Shevtsova, N.A., Busselberg, D., Molkov, Y.I., Bischoff, A.M., Smith, J.C., Richter, D.W., Rybak, I.A., 2014. Effects of glycinergic inhibition failure on respiratory rhythm and pattern generation. Prog. Brain Res. 209, 25–38.
Smith, J.C., Abdala, A.P., Borgmann, A., Rybak, I.A., Paton, J.F., 2013. Brainstem respiratory networks: building blocks and microcircuits. Trends Neurosci. 36, 152–162.
Smith, J.C., Abdala, A.P., Koizumi, H., Rybak, I.A., Paton, J.F., 2007. Spatial and functional architecture of the mammalian brain stem respiratory network: a hierarchy of three oscillatory mechanisms. J. Neurophysiol. 98, 3370–3387.
Smith, J.C., Ellenberger, H.H., Ballanyi, K., Richter, D.W., Feldman, J.L., 1991. Pre-Botzinger complex: a brainstem region that may generate respiratory rhythm in mammals. Science 254, 726–729.
Smith, J.C., Morrison, D.E., Ellenberger, H.H., Otto, M.R., Feldman, J.L., 1989. Brainstem projections to the major respiratory neuron populations in the medulla of the cat. J. Comp. Neurol. 281, 69–96.
St-John, W.M., Stornetta, R.L., Guyenet, P.G., Paton, J.F., 2009. Location and properties of respiratory neurones with putative intrinsic bursting properties in the rat in situ. J. Physiol. (Paris) 587, 3175–3188.
Stettner, G.M., Huppke, P., Brendel, C., Richter, D.W., Gartner, J., Dutschmann, M., 2007. Breathing dysfunctions associated with impaired control of postinspiratory activity in Mecp2-/y knockout mice. J. Physiol. (Paris) 579, 863–876.
Stettner, G.M., Zanella, S., Huppke, P., Gärtner, J., Hilaire, G., Dutschmann, M., 2008. Spontaneous central apneas occur in the C57BL/6J mouse strain. Respir. Physiol. Neurobiol. 160, 21–27.
Tan, W., Janczewski, W.A., Yang, P., Shao, X.M., Callaway, E.M., Feldman, J.L., 2008. Silencing preBotzinger Complex somatostatin-expressing neurons induces persistent apnea in awake rat. Nat. Neurosci. 11, 538–540.
Thoby-Brisson, M., Telgkamp, P., Ramirez, J.M., 2000. The role of the hyperpolarization-activated current in modulating rhythmic activity in the isolated respiratory network of mice. J. Neurosci. 20, 2994–3005.
Toporikova, N., Chevalier, M., Thoby-Brisson, M., 2015. Sigh and eupnea rhythmogenesis involve distinct interconnected subpopulations: a combined computational and experimental study. eNeuro 2015 (April (2)). https://doi.org/10.1523/ENEURO.0074-14.2015. pii: ENEURO.0074-14.2015, eCollection 2015 Mar-Apr.
Travers, J.B., Yoo, J.E., Chandran, R., Herman, K., Travers, S.P., 2005. Neurotransmitter phenotypes of intermediate zone reticular formation projections to the motor trigeminal and hypoglossal nuclei in the rat. J. Comp. Neurol. 488, 28–47.
Weber, F., Chung, S., Beier, K.T., Xu, M., Luo, L., Dan, Y., 2015. Control of REM sleep by ventral medulla GABAergic neurons. Nature 526, 435–438.
Wegener, E., Brendel, C., Fischer, A., Hulsmann, S., Gartner, J., Huppke, P., 2014. Characterization of the MeCP2R168X knockin mouse model for Rett syndrome. PLoS One 9, e115444.
Winter, S.M., Fresemann, J., Schnell, C., Oku, Y., Hirrlinger, J., Hulsmann, S., 2009. Glycinergic interneurons are functionally integrated into the inspiratory network of mouse medullary slices. Pflugers Arch. 458, 459–469.